


Article

# Experimental Study of Slamming Effects on Wedge and Cylindrical Surfaces

Byoungcheon Seo  and Hyunkyung Shin \*

School of Naval Architecture and Ocean Engineering, University of Ulsan, Ulsan 44610, Korea;  
inspectseo@naver.com

\* Correspondence: hkshin@ulsan.ac.kr; Tel.: +82-52-259-2696

Received: 22 November 2019; Accepted: 19 February 2020; Published: 22 February 2020



**Abstract:** Slamming is a very significant phenomenon that occurs in marine structures operating under extreme conditions. Slamming significantly reduces the design life of floating offshore wind turbines, as well as marine structures, and causes structural damage. Thus, the slamming load should be considered sufficiently during the design phase of the structure, and the results of experiments of good quality should be incorporated. The phenomenon of slamming should be analyzed using peak pressure, width, duration, and dynamic loads that depend on the design and natural frequency of the structure. In the case of a slamming experiment, the deadrise angle shows the greatest pressure between  $3^\circ$  to  $10^\circ$ . In this study, pressure values were compared using a model with a deadrise angle of  $10^\circ$  and a cylinder model most commonly used for the fabrication and installation of offshore structures. The peak pressure of the cylindrical model is greater than those of the flat model and the wedge model with a  $10^\circ$  deadrise angle. Pressure and strain were measured using free drops from heights of 1.0 and 1.7 m from the water surface, and the elastic effects were studied accordingly. Also, the peak pressure due to a slamming impact occurs several times depending on the natural frequency of the structure. In order to understand the behavior of the structure against the elastic effect, the second peak in the experimental results was theoretically and experimentally analyzed. The second pressure peak is greater than the first pressure peak due to the elastic behavior effects based on the natural frequency of models used in the slamming test. Also, a single slamming results in several peak pressures and it greatly deteriorates the fatigue strength. Experiments and simulations were carried out to derive the effects of repeated slamming loads on the structure. In the structural design considering the slamming loads, information on the elastic effect of the structure and accumulated loads is very important. This can be an important variable in the design of the floater and can play an important role in assessing the impact on the floater. These results raise questions as to the extent that slamming pressures are replaced with equivalent hydrostatic pressures in most design rules of the recognized certification society.

**Keywords:** slamming phenomena; impulse; duration; peak pressure; free-drop test; deadrise angle

## 1. Introduction

Offshore structures suffer from various types of impulsive pressure loading, such as slamming, sloshing, and green water. Most studies have focused on estimating the slamming pressure and maximum pressure accordingly [1]. Based on the peak pressure, the slamming load is calculated as the equivalent design pressure. According to the results of several studies, not only the peak pressure but also the duration of pressure play an important role in predicting the range of damage to the structure [2].

Figure 1 shows the structural damage caused by slamming loads when the marine structure operates in extreme conditions. The slamming impact load may be described by the magnitude of the

load, rise time, and duration. The phenomenon of slamming is strongly nonlinear and affected by the behavior and shape of the structure. Severe pressure due to slamming can be exerted on floating offshore wind turbines and could exacerbate their structural damage and deteriorate their strength.

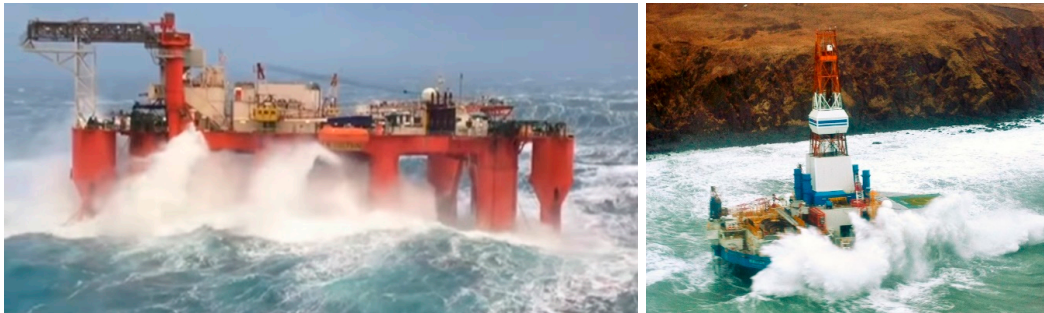


**Figure 1.** Structural damage caused by slamming in extreme conditions.

The authors of [3] conducted a repeated drop experiment using a bottom model of a ship with a deadrise angle of  $10^\circ$ . The central deformation was measured after each test, and, in most classifications, the slamming impact pressure was assumed to be static and the dynamic nature was ignored.

The basis of this assumption was that the duration of the impact pressure was greater than the natural frequency of the impacted structure, as reported by the authors of [3]. A free-drop experiment using a steel model was performed to determine the effects of elasticity on the slamming pressure. The slamming pressure was measured within a very short time as the test model was dropped freely onto the water surface [4]. The first pressure measured is due to slamming and the second pressure is due to the interaction with the natural frequency of the structure. The second pressure was large enough to not be ignored compared to the first pressure.

In general, when the duration of non-dimensional pressure is less than 1, the behavioral characteristics of the structure are determined by the impulse values, regardless of peak pressure and duration. Conversely, when the duration of non-dimensional slamming pressure is greater than 1, the behavioral characteristics of the structure are determined by the peak pressure.

However, if the duration of the pressure is similar to the natural frequency of the structure, the behavioral characteristics of the structure are affected by both peak pressure and duration [5,6]. Even a single wave acting several times leaves permanent deflections over the impacted region. Meanwhile, [7–9] and [10] included structural damage due to slamming. In this paper, the inverse of the duration of pressure was compared with the natural frequency of the structure. Therefore, units for both parameters are the same as Hz.

Recently, as the importance and interest in renewable energy has increased, further research has been conducted into installing wind turbines at sea. Korea's offshore wind turbines have excellent geographical conditions. The Yellow Sea, with low water depth, is favorable for the construction of fixed wind turbines. The East Sea, with a relatively high-water depth, is favorable for the installation of floating wind turbines and facilitates the creation of large-scale complexes.

In the case of offshore wind turbines, many types of technical aspect should be considered before design. Among these, damage to the structure caused by slamming loads should be investigated. According to recently published papers and case studies, design life in the context of structural damage due to slamming loads is being actively investigated.

Figure 2 shows the presence of slamming loads on a 1:40-scale floating offshore wind turbine model during experiments under irregular wave conditions. As shown in Figure 2, the floating wind turbines experience bottom slamming, wave run-up slamming, and horizontal slamming. Under these conditions, certain combinations of slamming loads can be harmful. Hull vibrations can be induced temporarily through the frame of the structure [4]. In the case of floating production, storage and offloading, all employees are evacuated owing to the damage caused by slamming loads [11]. This

indicates the need for a dynamic approach to account for this phenomenon. Under these conditions, it can be questioned whether the dynamic characteristics of slamming loads can be ignored and handled statically. Analyses and numerical studies [12] on slamming have been conducted for several decades and efforts have been made to apply these to various phenomena of slamming—wedge and cone [13–15], cylinder [16–18] and flat [19,20]. Furthermore, experimental studies were conducted to confirm the phenomenon of slamming. In this study, the slamming load characteristics and elastic effects are investigated by using a model with a deadrise angle of  $10^\circ$  and a cylindrical model dropped freely from heights of 1.0 and 1.7 m, and the effect of slamming on the structure is examined.

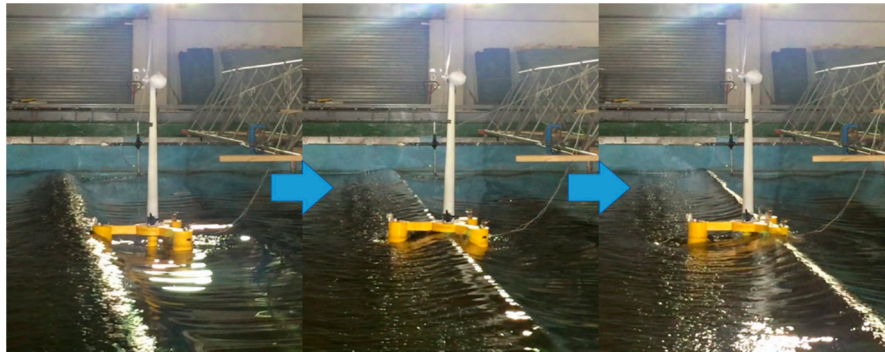


**Figure 2.** Floating offshore wind turbine model experiment in the University of Ulsan’s ocean engineering wide tank.

## 2. Experimental Conditions

### 2.1. Experiment Set-Up

All the experimental data were recorded in very short durations of time, and obtaining correct results was one of the most important tasks. The selection of the experimental equipment and method, and the measurement of experimental data, are very important. Therefore, this section focuses on the equipment, method, and measurement in detail. As shown in Figure 3, the free-drop test was conducted using a free-drop experimental device in the ocean engineering wide tank, University of Ulsan, Ulsan, Korea.

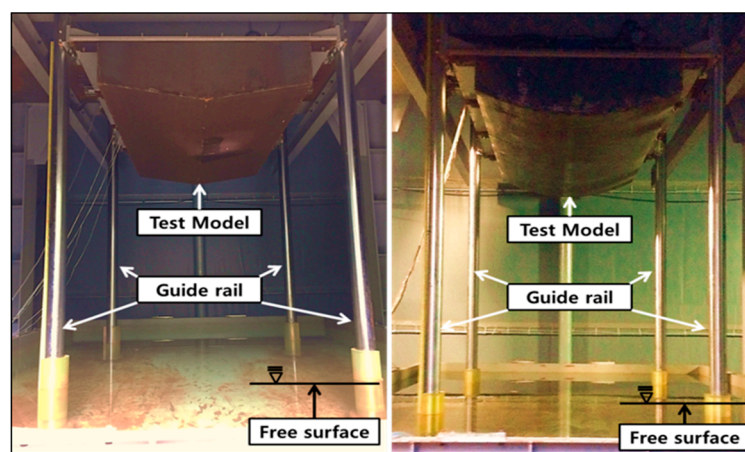


**Figure 3.** Installed model with deadrise angle of  $10^\circ$  (left) and cylindrical model (right) in slamming test system.

### 2.2. Experimental Test Loop

Figure 4 shows the slamming experimental test set-up condition. The experimental model begins to drop freely at the same time at which the current of the electromagnet is cut. The measurements of the pressure sensors and strain gauges are synchronized and stored at 100 kHz/s, together with the signal of cutting the current of the electromagnet. As the sampling rate effect and comparison of pressure sensors are checked before the free-drop test, the experimental set-up is deemed perfectly installed.

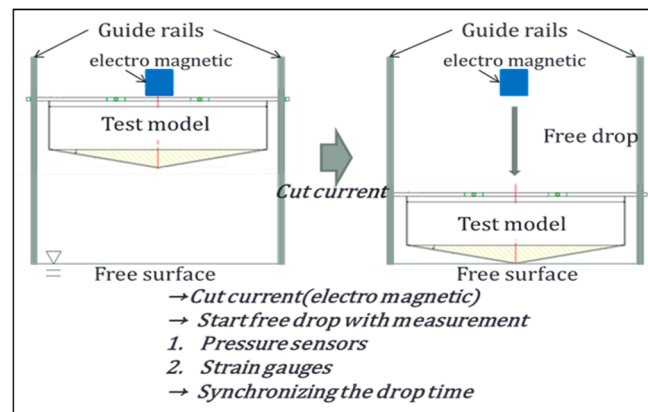


Figure 4. Slamming experimental test set-up condition.

As shown in Table 1, the free drop heights of each model are 1.0 and 1.7 m. At the heights of 1.0 and 1.7 m, the bottom thickness of each model was varied to 3, 5 and 8 mm.

Table 1. Free drop test conditions.

Model Shape	Free Drop Height [m]	Bottom Thickness [mm]
Dead rise angle 10°	1.0, 1.7	3, 5, 8
Cylindrical		

The frame of the machine was 3.5 m long, 4.0 m wide, and 5.0 m high, and the water tank was 4.0 m long, 3.0 m wide, and 1.0 m deep. The test model was lifted to a set height using hydraulic pressure. The test model and slamming test device were secured using an electromagnet. The maximum drop height of the slamming test facility was 1.7 m, and the free-drop test was performed by blocking the current in the electromagnet. Four vertical guide rails were used to keep the test model’s bottom parallel to the water plane before the model enters the water. Two safety bars were installed to account for the unexpected current interruption.

### 2.3. Locations of the Sensors

The physical values measured in this experiment are pressure and strain. As shown in Figure 5, eight pressure sensors and three strain gauges were installed. The pressure sensors were installed horizontally and vertically with respect to the center to characterize the phenomenon of slamming. The positions of the pressure sensors are indicated in blue and those of the strain gauges are indicated in orange. The pressure sensor P1 was the first to be subjected to slamming pressure. P7 and P8 were placed on the same line as P1 and P2 to ensure that the test model dropped horizontally to the free surface.

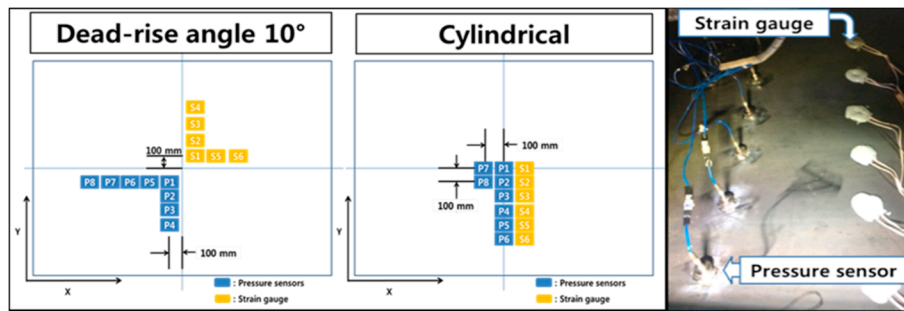


Figure 5. Locations of the sensors.

### 2.4. Pressure Sensors

The piezoelectric sensors are characterized by large resonance frequencies and short response times, which are necessary for measuring the slamming pressure. Typically, the sensors have response times in the order of microseconds and resonance frequencies in the order of hundreds of kHz. The pressure sensor diaphragm was installed horizontal to the bottom surface of the model, as described by [21]. The sensors used in this paper have resonance frequencies higher than 500 kHz [22]. The sensitivity value of the pressure sensor was used to set and calibrate the initial value, listed in Table 2.

Table 2. Sensitivity of pressure sensors.

Sensor Number	Voltage Sensitivity	
1	4.967 mV/PSI	720.4 mV/Mpa
2	5.043 mV/PSI	731.5 mV/Mpa
3	5.044 mV/PSI	731.6 mV/Mpa
4	4.963 mV/PSI	719.8 mV/Mpa
5	5.047 mV/PSI	732.0 mV/Mpa
6	4.963 mV/PSI	719.8 mV/Mpa
7	5.067 mV/PSI	734.9 mV/Mpa
8	5.061 mV/PSI	727.5 mV/Mpa

### 2.5. Strain Gauges

The electrical resistance method was applied to measure the strains. The material properties were defined by employing the equations proposed by [8]. For the strain gauge, two channels were used, and the strains in the x and y directions were simultaneously measured. Table 3 lists the specifications of the strain gauge. The strain gauge resistance values and factors were used to set and calibrate the initial values.

Table 3. Specification of strain gauge.

Gauge Length	Gauge Factor	Gauge Resistance
6 mm	1 = 2.10, 2 = 2.10, ±1%	120 ± 0.5 Ω

### 2.6. Data Acquisition System with Calibrations

Figure 6 shows the calibrations of the NI PXI data acquisition system that was used to acquire and process the measured data. It is a multichannel data acquisition system and industrial computer. At high streaming rates, it provides real-time data for waveform and gauge displays with unlimited recording duration and file size. The data were stored by synchronizing the drop times. In this experiment, the pressure and strain were measured at 100 kHz/s for each sensor and strain gauge. Pressure peaks occur in very short periods of time in slamming experiments. Therefore, an appropriate sampling rate should be set so that the information can be measured without being distorted. The calibration of the

sensor was performed by entering the information from Tables 2 and 3. Each sensor had the same specification, but the sensitivity was slightly different.

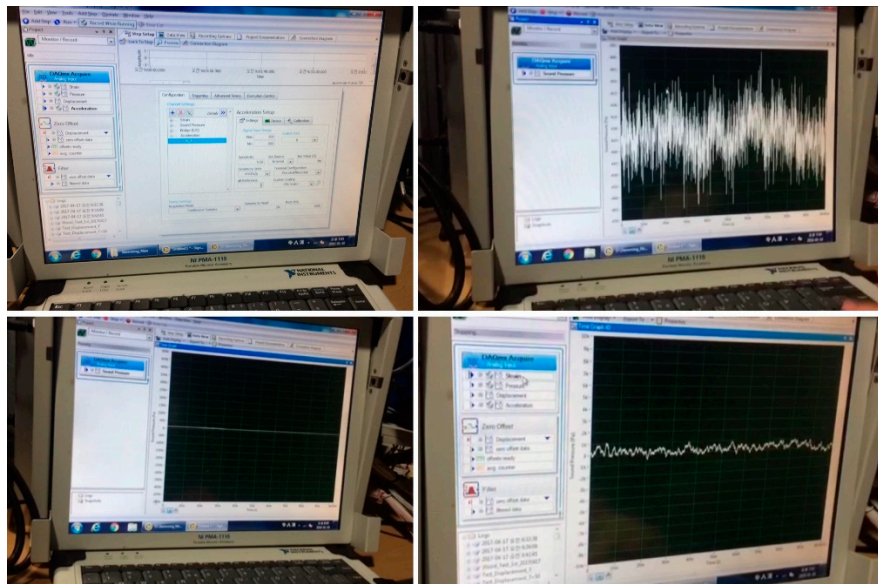


Figure 6. Sensors calibration and data measuring rate set before free drop test.

### 2.7. Dimensions of Test Models

Details of the models used are listed in Table 4. The model used in the experiment was made of mild steel (Class SS41), which is a general-purpose structural steel.

Table 4. Dimensions of the test models.

Material	Steel	
Deadrise angle [°]	Cylindrical	10
Length [m]	2.00	
Width [m]	1.20	
Height [m]	0.28	
Mass [kg]	340	
Bottom wedge thickness [mm]	3, 5, 8	

Figure 7 shows a sectional feature of the model with a deadrise angle of 10°. It was 1.2 m in width, 2.0 m in length, and 0.3 m in height. The model had a mass of 340 kg and thickness of 3, 5 and 8 mm.

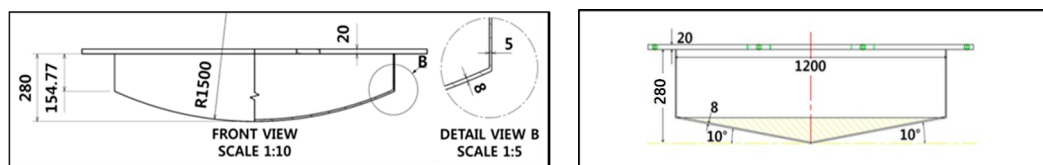


Figure 7. Sectional geometry of the cylindrical model with a deadrise angle of 10°.

Figure 7 shows a sectional feature of the model with cylindrical shape. It was 1.2 m in width, 2.0 m in length, and 0.28 m in height. The model had a mass of 340 kg and thickness of 8 mm, identical to those of the model with a deadrise angle of 10°.

### 2.8. Tensile Test

The material used in the tests was mild steel (SS41 grade), which is commonly used in marine structures. Tensile strength tests were conducted using certified specimens and tester in accordance with the specifications provided by the [23].

Tensile coupons were tested, and the averages of the mechanical properties were obtained from actual tensile tests; the yield stress is 280 MPa, as shown in Figure 8 and Table 5. The values of the pressure used in the simulations were obtained from the actual experimental results.

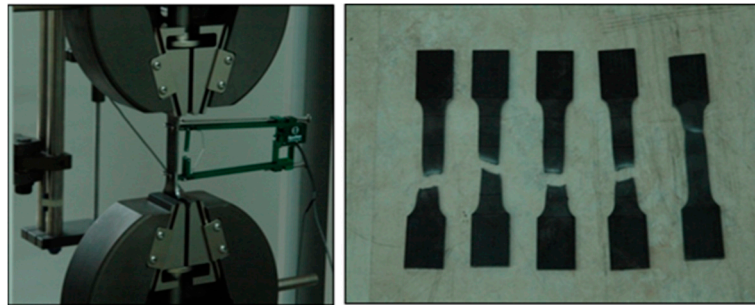


Figure 8. Tensile test specimen of the same material as that of the model used in the experiment.

Table 5. Tensile test results.

Thickness		Yield Stress	Ultimate Strength
Nominal [mm]	Actual [mm]	[MPa]	[MPa]
8.0 mm	7.9	280.8	433.2

### 3. Experimental Results for Model with Deadrise Angle of 10° and Cylindrical Model

It seems that the second peak pressure occurs when the negative pressure, due to the elastic effect, was close to  $-0.1$  Mpa.

Figures 9 and 10 show that the second peak was larger than the first peak in the wedge models. However, in the case of the cylinder models, except for the bottom thickness of 3 mm, which is largely deformed, the size of the second peak was smaller compared to the first peak.

As the bottom thickness increases, the pressure tends to increase. In the case of the bottom thickness of 3 mm, in which deformation occurs, the pressure history shows that the fluctuation of the shape of the pressure was very large and it persists. In the case of slamming loads, the peak pressure and the duration of it are important factors. Longer durations along with peak pressures indicate longer and high loads on the structure.

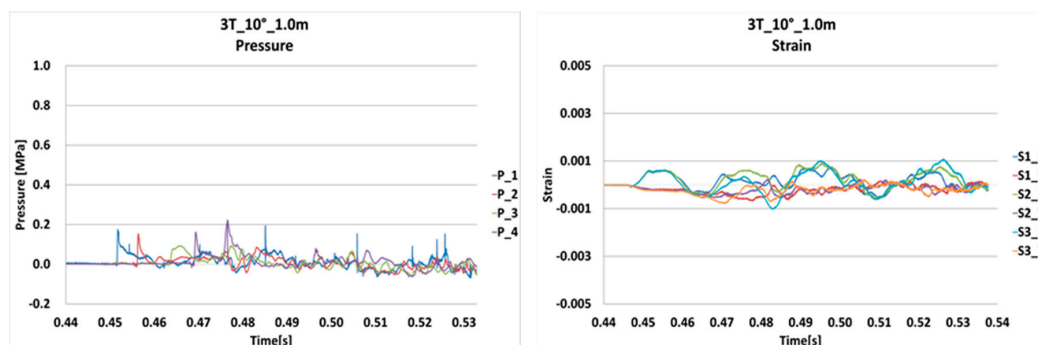


Figure 9. Cont.

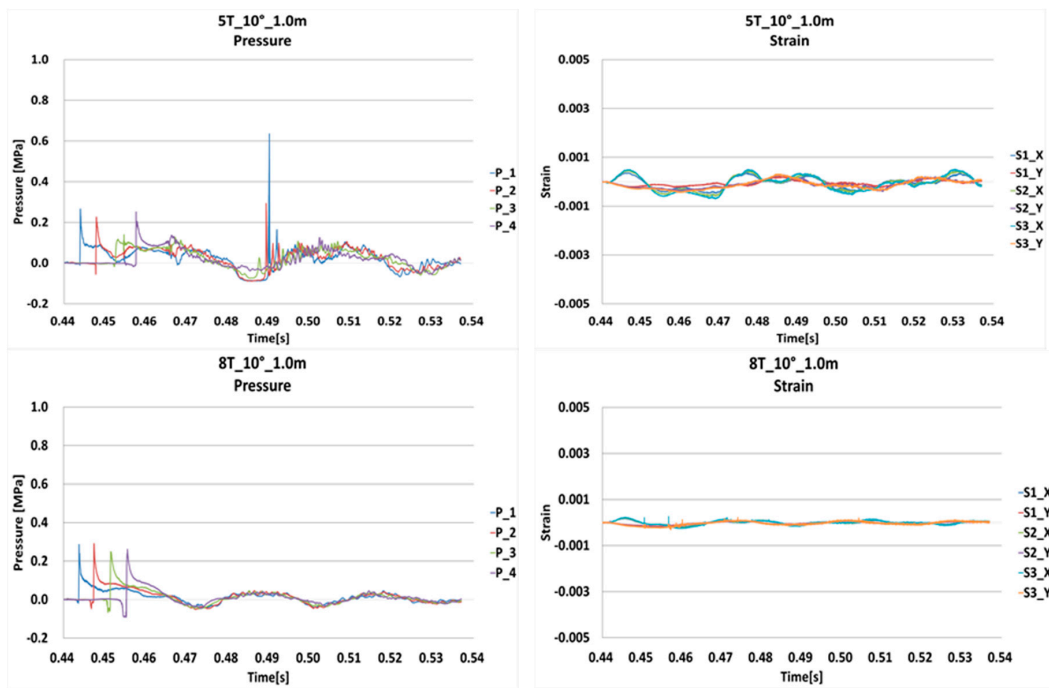


Figure 9. History of pressure and strain in the model with deadrise angle of 10° (Drop height: 1.0 m).

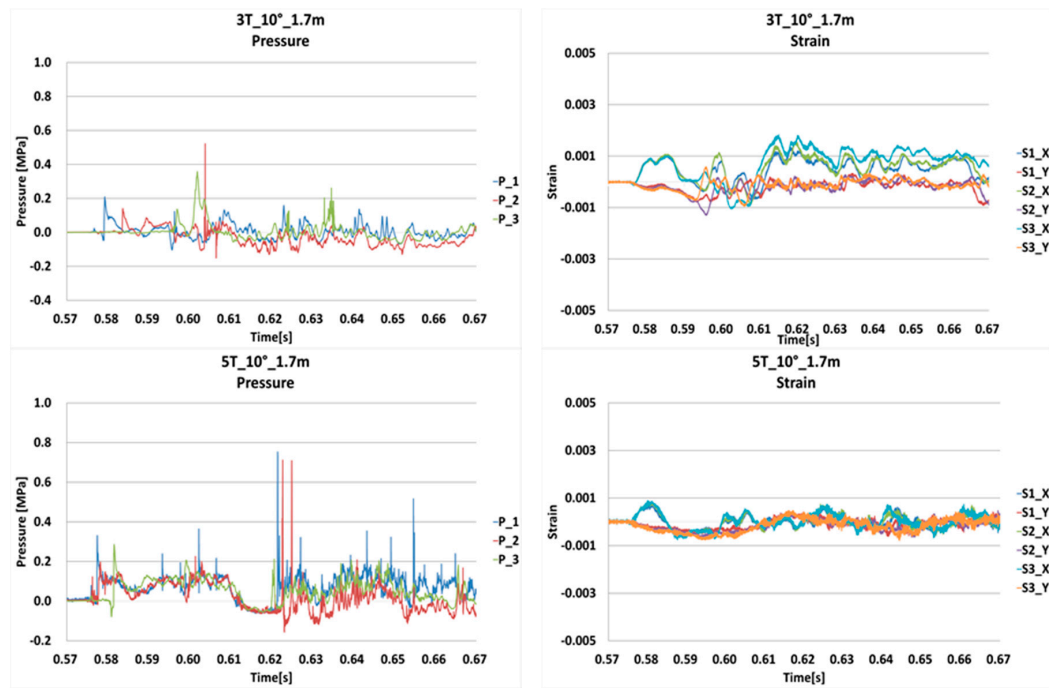


Figure 10. Cont.



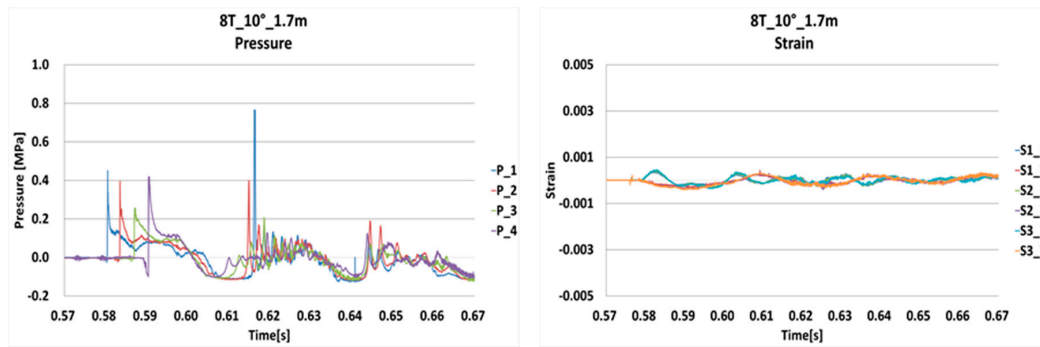


Figure 10. History of pressure and strain in the model with deadrise angle of 10° (Drop height: 1.7 m).

Figures 11 and 12 show that the strain history does not converge to zero, when the impact was applied and deformation occurs, the second peak due to the elastic effect was confirmed to be larger or similar to the first peak.

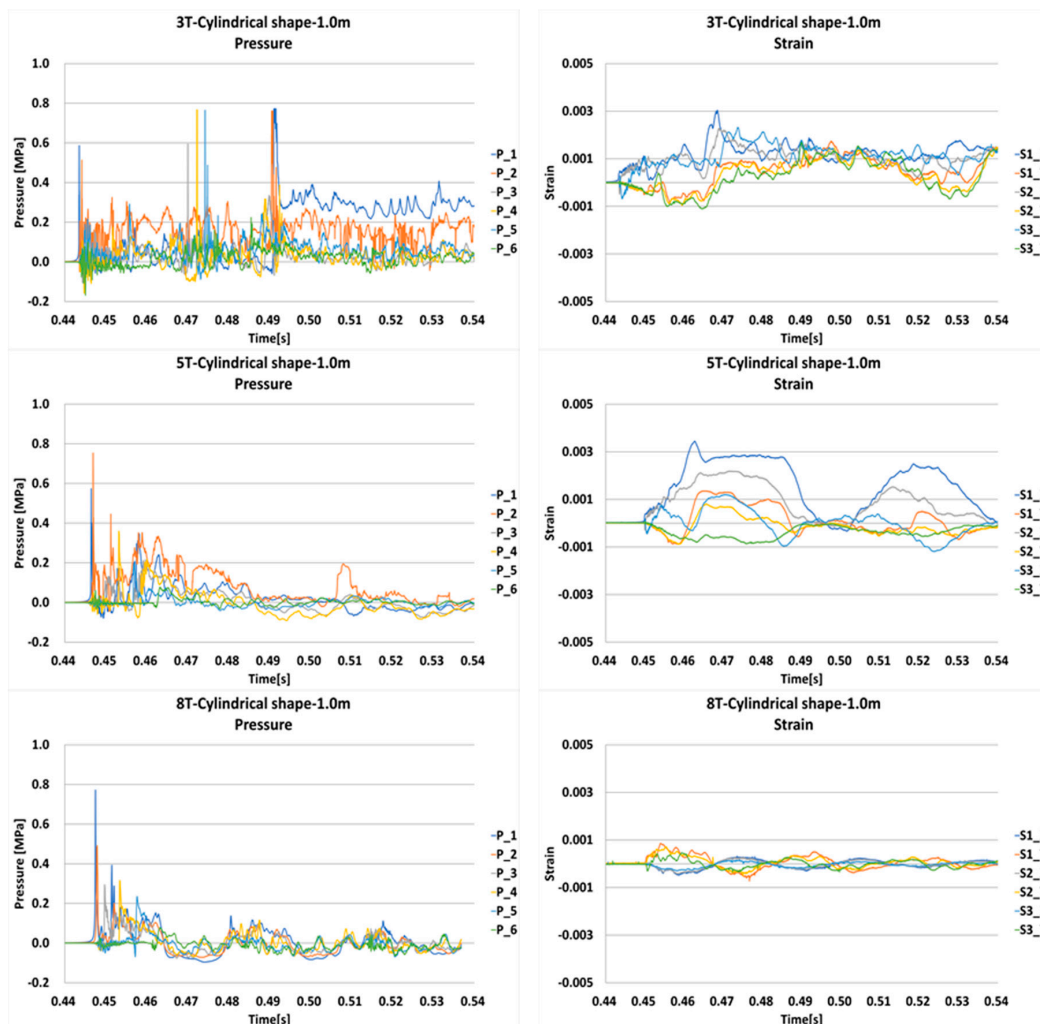


Figure 11. History of pressure and strain in the model with cylindrical shape (Drop height: 1.0 m).

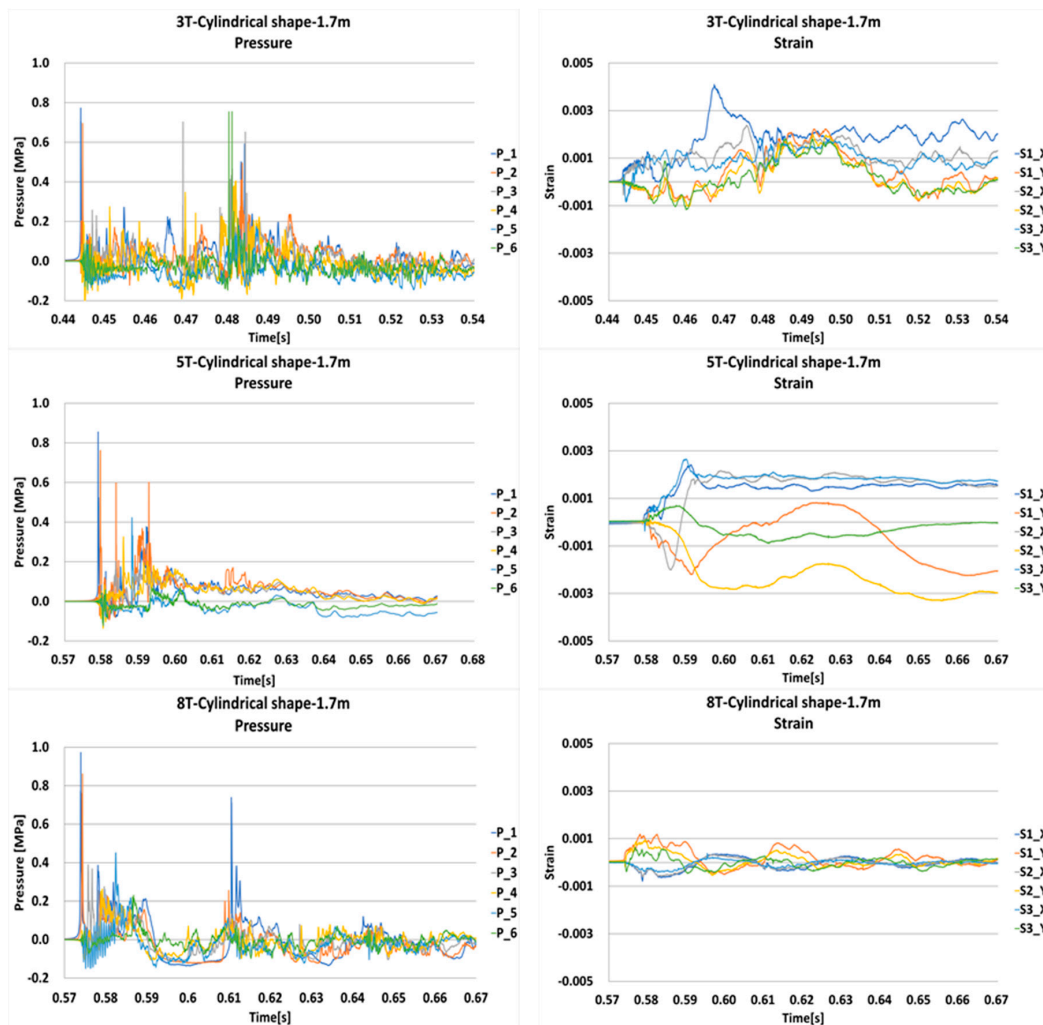


Figure 12. History of pressure and strain in the cylindrical model (Drop height: 1.7 m).

It seems that the negative pressure occurred due to the elastic influence of the structure. Figure 13 shows that the negative pressure of the rigid model, made of wood, was negligible. On the other hand, in the case of the elastic model, made of steel, negative pressure was confirmed, as shown in Figures 11 and 12.

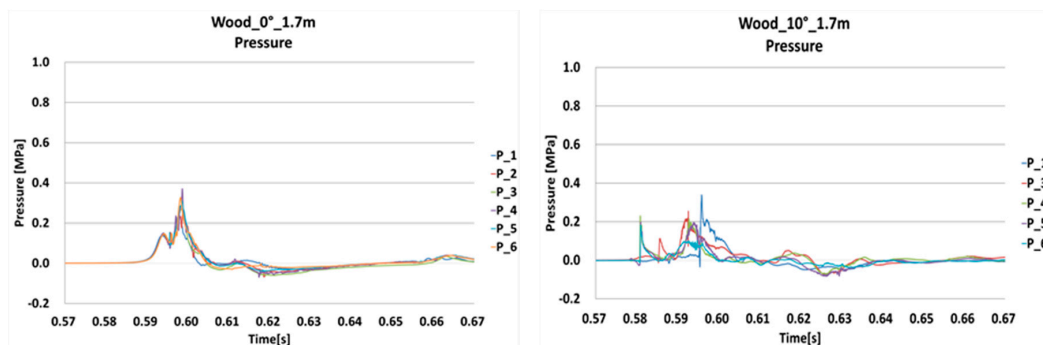
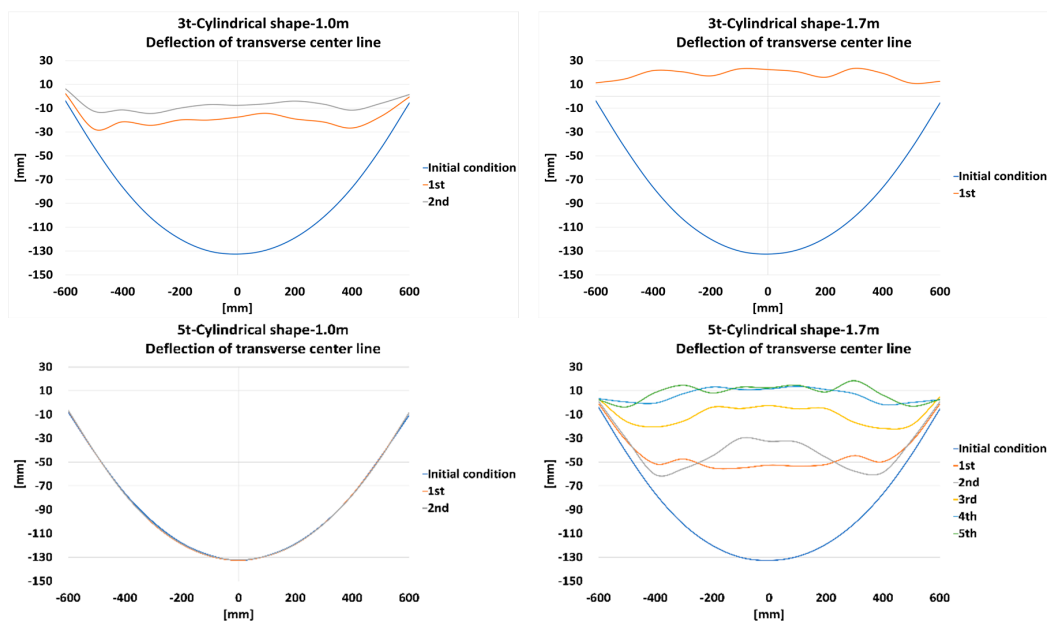


Figure 13. History of pressure in the wooden wedge model with a deadrise angle of 0° and 10° (Drop height: 1.7 m).

As shown in Figure 14, when the bottom thickness was 3 mm, deformation occurred at both 1.0 and 1.7 m drop heights. Figure 14 shows the strain measured after repeated drop tests. At the

bottom thickness of 8 mm, no deformation occurred, so it is omitted. The deformations for the models with bottom thicknesses of 5 and 3 mm were measured and plotted. The deformation was measured by measuring the center cross section of the model, and each deformation is shown in Figure 14. Deformation did not occur when the bottom thickness was 5 mm and the drop height was 1.0 m, and deformation occurred when the height was 1.7 m. The deformation was measured by performing five-time free drops, and the maximum deformation of the central section was up to 140 mm. The model with a bottom thickness of 3 mm was deformed at both 1.0 and 1.7 m. Deformation was measured twice at the drop height of 1.0 m, and the maximum deformation of the central cross section occurred up to 140 mm. Due to the high degree of deformation of the model, no additional drop test was possible. At 1.7 m drop height, the maximum deformation of the central section was measured to be more than 150 mm. The model was so deformed that further drop tests were not possible.



**Figure 14.** Deflection curves from consecutive drop tests at cylindrical model (height: 1.0, 1.7 m, bottom thickness: 3, 5 mm).

## 4. Hammering Test

### 4.1. Methodology

The impact hammering test was performed to compare the behavioral characteristics of the structure at the pressure sensor locations with those obtained from the numerical simulation. The natural frequency of the structure was measured using an accelerometer, a shock hammer, and a vibration analyzer (Fast Fourier Transform analyzer). SignalCalc-ACE was used to synchronize the signals of the impact hammer and accelerometer. Furthermore, the experiment was performed under the assumption that all four sides of the structure were fixed.

The average result of five impacts was obtained for each case. The results were also checked for signal quality (adequate signal-to-noise) and the absence of overloads (overload lights or sharp flattening of time history peak) and double impacts. The electrical and mechanical connections were checked during each test, as they tend to become loose from repeated impacts.

$$T_n = \frac{1}{f_n} \tag{1}$$

where

$$f_n = 5.544 \times \frac{t}{ab} \sqrt{\left(\frac{a}{b}\right)^2 + \left(\frac{b}{a}\right)^2} + 0.6045 \tag{2}$$

*a* and *b* are the longer and shorter lengths of the plate, respectively.

#### 4.2. Results for Model with Deadrise Angle of 10° and Cylindrical Model

The values of natural frequency obtained from theoretical calculation using Equation (2), free-drop experiment, and hammer test are listed in Table 6. Figures 10, 12 and 15 show that the experimental values obtained via the hammering test are 34.1 Hz and 35.5 Hz in the case of the model with a deadrise angle of 10° and the cylindrical model, respectively, as listed in Table 6.

**Table 6.** Natural frequency from theoretical calculation, free-drop test, and hammer test.

	In Air [Equation (2)] [Theoretical]	Experimental [Drop Test]	Experimental [Hammer Test]
Deadrise Angle 10°	34.8 [Hz]	33.3 [Hz]	34.1 [Hz]
Cylindrical	34.1 [Hz]	33.3 [Hz]	35.5 [Hz]

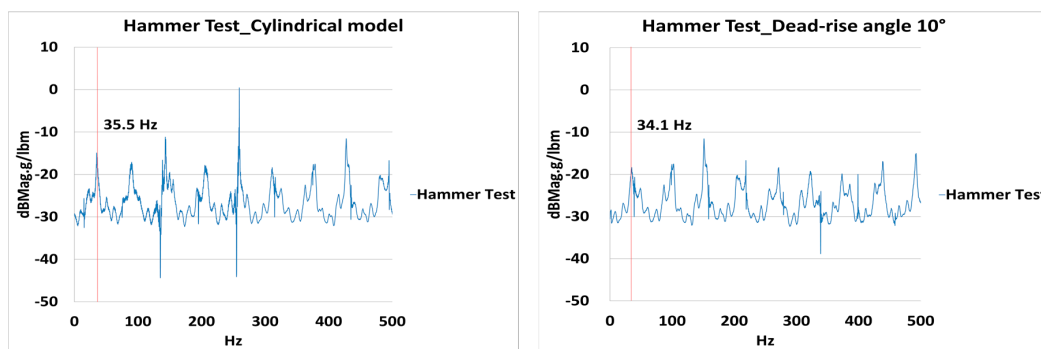


**Figure 15.** Hammering test result for cylindrical model (left) with deadrise angle of 10° (right).

It can be confirmed that the theoretical and experimental values are almost identical. The slight difference appears to be due to the fact that the test model is interlocked with the test equipment and their boundary conditions. The second pressure peak is greater than the first pressure peak due to the elastic behavior effects based on the natural frequency of models used in the slamming test. Also, a single slamming results in several peak pressures and it greatly deteriorates the fatigue strength.

## 5. Numerical Simulation

### 5.1. Methodology

Numerical simulations were performed using the nonlinear package of ABAQUS software (Abaqus, Version 6.14) for comparison with the experimental results. The impulsive pressure loadings obtained from the actual free-drop tests were used as input data for the simulations. The elastic cylindrical test model was used for the experiments as well as numerical simulations.

Figure 16 shows that the cylindrical test model was modeled using the four-node shell element (S4R) from the ABAQUS element library. Five integration points were used through the thickness, and the default values of hourglass controls were used for this element. Convergence simulation was performed for several mesh sizes. The mesh sizes of each test model were determined to be approximately five times its thickness, as shown in Figure 16.

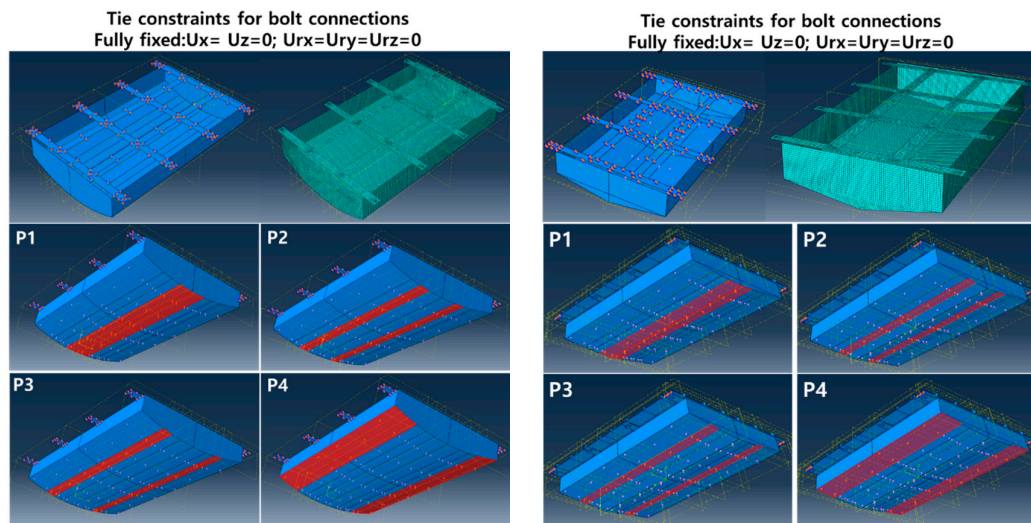


Figure 16. Finite element model of the cylindrical model (left) with deadrise angle of 10° (right).

The contact between the test model and support frame was expressed using the “surface-to-surface contact” option from the in-contact library employed in ABAQUS. The penalty and “hard” contact methods were used to define the tangential and normal interaction behaviors of any possible self-contact among the model parts during impact. The friction coefficient between the model and support frame was set at 0.2, as proposed by [24]. The acting pressure value was obtained from the experiment, and the time of pressure acting differed from P1 to P4, as shown in Figures 5 and 16.

The test model and the frame to which it is connected are modeled to be fully fixed, as is the case with the actual experiment. As shown in Figure 16, the top of the model was modeled to be in a fully fixed state, and a tie contrast technique was used to achieve this.

### 5.2. Numerical Prediction Results for Model with Deadrise Angle of 10° and Cylindrical Model

Nonlinear dynamic analysis was performed using ABAQUS tool. Figure 17 shows the result of the comparison between the experiment and numerical simulation in terms of strain. It was confirmed that the results obtained from the experiment are consistent with those obtained from the numerical simulation. The measurement point of strain was the point of S1, as shown in Figure 5, which is located 100 mm, in the both horizontal and vertical directions, from the center. The result of the simulation is also the strain result at the same location.

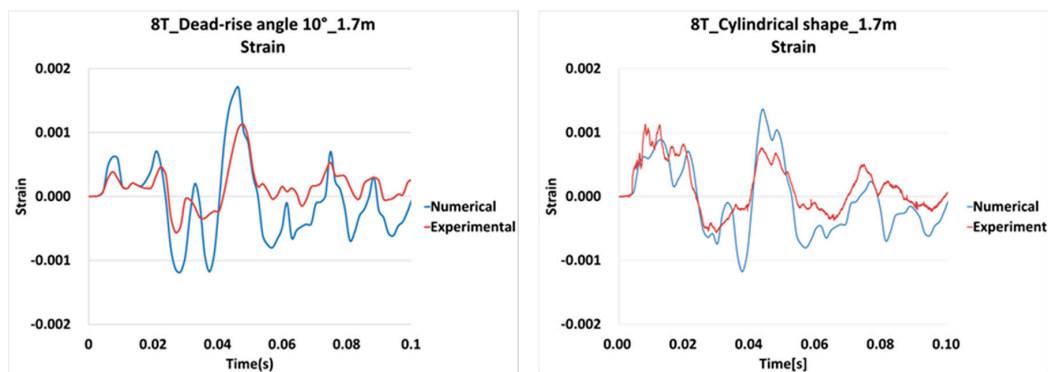


Figure 17. Comparison of strain values obtained from experimental results and numerical simulation.

### 5.3. Comparison of Simulation and Experimental Results for the Accumulative Damage of Cylindrical Model

In order to investigate the accumulative damage, the model with a bottom thickness of 5 mm was subjected to five free drop tests. Five accumulative pressures were applied to compare the results of the simulation with the cumulative strain from five free drop tests.

The simulation results are shown in Figure 18. The deformation at the first impact was 100 mm, which was about 20 mm larger than the deformation obtained in the actual experiment. However, the deformation at the last (fifth) impact is 145 mm, showing a slight error of about 5 mm from the experimental value.

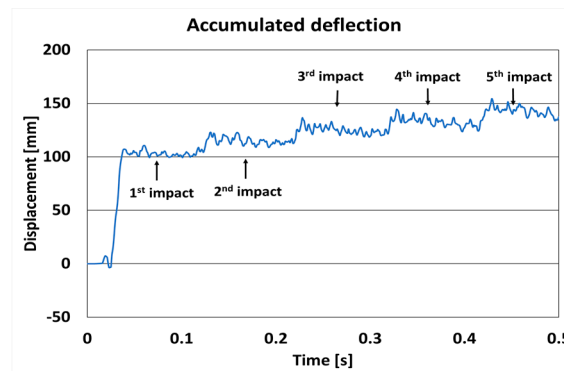


Figure 18. Accumulated deflection result for simulation.

In addition, simulations show a constant increase in deformation, and the experimental value can confirm the tendency of the deformation by the continuous impact load to gradually decrease compared to the initial deformation.

Table 7 shows the deformation amounts in the experiments and simulations. Figure 19 shows strain measurements for the first and fifth experiments.

Table 7. Max. Displacement at center line.

	1st	2nd	3rd	4th	5th
Measurement [mm]	80	100	120	130	140
Simulation [mm]	105	115	125	135	145

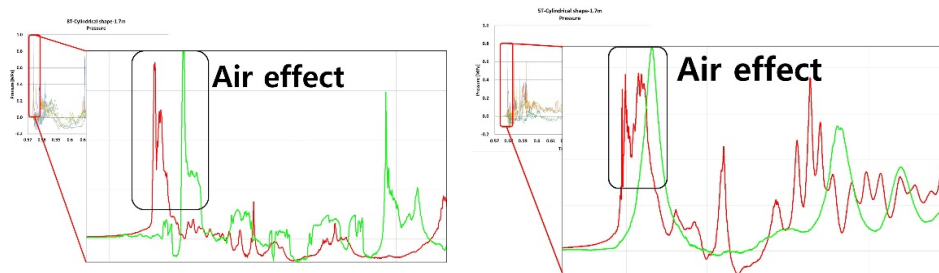


Figure 19. Measurement of the 1st free drop test (left) and the 5th free drop test (right).

## 6. Results and Discussion

As shown in Figure 20, the air effect phenomenon appeared in the cylinder shape as well as the flat model. This acts as a deterrent to the increase in pressure. In general, slamming pressure is highest when the dead-rise angle is 3 to 10 degrees. It was confirmed from the pressure history that the air

effect, such as in the flat shape at the thickness of the cylinder shape and a bottom thickness of 5 and 8 mm, occurs.



**Figure 20.** Air effect at a bottom thickness of 5 and 8 mm in cylindrical shape model.

Also, Figure 20 shows an enlarged pressure history of a cylindrical shape model. It seems that the pressure shape of the enlarged graph shows two peaks due to the air effect. As with the flat shape, it does not reach the maximum pressure and shows the effect of dispersion.

Figure 9 shows the pressure and strain time history of the free-drop test of the model with a deadrise angle of  $10^\circ$  dropped from a height of 1.0 m. It confirms that the time at which the pressure was generated differs according to the angle formed by the deadrise angle, and that the strain exhibits the same behavioral characteristics. This means that the elastic period of the elastic body coincides with the natural frequency. Figure 10 shows the pressure and strain time history of the free-drop test of the model with a deadrise angle of  $10^\circ$  dropped from a height of 1.7 m. The characteristics of the natural frequency of the structure are more clearly shown in Figure 10. At 0.585 s, the first peak pressure was generated due to the free-drop impact, and the second peak pressure and the third peak pressure are confirmed at approximately 0.625 and 0.655 s, respectively, i.e., after 0.03 s. This is indicated by a red square in Figure 10. The behavior of the strain oscillation was confirmed to be very similar to that of the pressure history.

Figure 11 shows the pressure and strain time history of the free-drop test of the cylindrical model dropped from a height of 1.0 m. It confirms that strain exhibits the same behavioral characteristics as pressure history does. This means that the elastic period of the elastic body coincides with the natural frequency. Figure 12 shows the pressure and strain time history of the free-drop test of the cylindrical model dropped from a height of 1.7 m. The characteristics of the natural frequency of the structure are more clearly shown in Figure 12. At 0.60 s, the first peak pressure was generated due to the free-drop impact, and the second peak pressure was confirmed at approximately 0.63 s, i.e., after 0.03 s. This is shown in a red square in Figures 10 and 12. The behavior of the strain oscillation was confirmed to be very similar to that of the pressure history.

Figure 20 and Table 8 show the pressure time history and impulse values measured in the free-drop experiment of the model with a deadrise angle of  $10^\circ$  and the cylindrical model. The highest value of pressure was measured in the cylindrical model relative to the flat model and the model with a deadrise angle of  $10^\circ$ . In the case of the model with a deadrise angle of  $10^\circ$ , the maximum pressure when dropped from a height of 1.0 m was 0.29 MPa, with a maximum strain of 0.0010, and the maximum pressure when dropped from a height of 1.7 m was 0.45 MPa, with a maximum strain of 0.0010. In the case of the cylindrical model, the maximum pressure when dropped from a height of 1.0 m was 0.78 MPa, with a maximum strain of 0.0010, and the maximum pressure when dropped from a height of 1.7 m was 0.98 MPa, with a maximum strain of 0.0012. Slamming pressure and strain were shown to increase with drop height and thickness by [25]. When the deadrise angle of the model decreases, the slamming pressure increases. Elastic effects should be considered when the deadrise angle is less than  $6^\circ$  [26].

**Table 8.** Peak pressure, duration, and impulse for the cylindrical model and model with deadrise angle of 10° at first peak pressure.

Model Shape	Drop Height (m)	Bottom Thickness (mm)	Peak Pressure (kPa)	Duration (s)	Impulse (kPa·s)
Deadrise angle of 10°	1.0	3	170	0.0010	0.085
		5	250	0.0010	0.125
		8	290	0.0010	0.145
	1.7	3	200	0.0010	0.100
		5	320	0.0010	0.160
		8	450	0.0010	0.225
Cylindrical	1.0	3	580	0.0015	0.435
		5	750	0.0020	0.750
		8	780	0.0020	0.585
	1.7	3	770	0.0015	0.578
		5	850	0.0020	0.850
		8	980	0.0020	0.980

The rate of increase in strain was very small compared to the rate of increase in pressure. Figures 10 and 12 confirm the occurrence of the first peak and the second peak, approximately 0.03 s later. The second peak pressure was an occurrence caused by the effects of the structure's natural frequency. The natural frequency of an unstiffened plate can be estimated using Equation (1), the natural frequency of the plate is obtained from Equation (2), as proposed by [27], and the natural frequency can be obtained from its reciprocal.

Figure 13 provides the basis for supporting the previous claim. Figure 13 shows the pressure time history of the free-drop test of the model with a deadrise angle of 10° dropped from a height of 1.7 m. The pressure values were measured in an experiment using wood, which is assumed to be rigid. When a wooden specimen was employed in the experiment, the second peak pressure seen in the elastic models could not be confirmed. This means that in the estimation of the slamming pressure of an object with elastic effects, the natural frequency of the structure must be considered.

In order to prove the absence of the influence of reflected waves, a number of experiments were conducted in which a test apparatus was set up so that the influence of the reflected waves was not affected. At the time, however, it was confirmed that a second peak occurred.

The results obtained by [28] from experiments using models with deadrise angles of 0° and 10° show the same tendency in the case of pressure coefficient. However, the slamming pressure coefficient was the highest when the deadrise angle was 3° and was not influenced by the air effect observed when the deadrise angle was 0°.

Figure 21 shows a simplification of the slamming pressure. The peak pressure (P1) and its duration ( $t_1$ ) can be used to determine the triangular shape of the impulse value, as described by [29]. The values of peak pressure and duration obtained from the free-drop experiments are shown in Table 8. The impulse values are obtained by idealizing peak pressure and duration, as shown in Figure 21; when the deadrise angle was 10°, the duration tended to remain the same, even as the peak pressure increased. However, an experiment with the cylindrical model confirmed that duration increased with pressure.



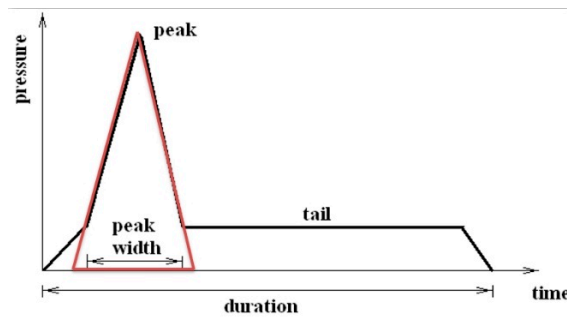


Figure 21. Simplified triangular pressure.

Figure 22 compares the maximum pressure values of the cylindrical model, flat model, and the model with a deadrise angle of 10°. In the case of the model with a deadrise angle of 0°, the maximum values of pressure measured, when drop heights were 1.0 and 1.7 m, were 0.19 and 0.33 MPa, respectively, according to [5]. In the case of the model with a deadrise angle of 10°, the pressure values, when drop heights were 1.0 and 1.7 m, were 0.29 and 0.45 MPa, respectively, according to [25]. Finally, the largest pressure value was obtained in the case of the cylindrical model. The pressure, when drop heights were 1.0 and 1.7 m, was measured to be 0.78 and 0.98 MPa, respectively. Comparing the impulse values, the cylinder shape was found to be about four times larger than the model with the dead-rise angle of 10 degrees. This means that the cylinder shape, which is widely used in offshore structures, is more affected by slamming loads.

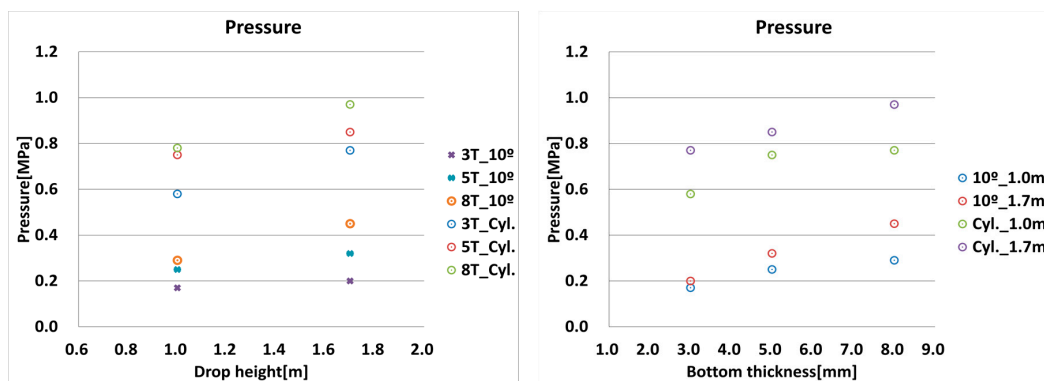


Figure 22. Comparison of peak pressures.

Table 8 listed the impulse value calculated by idealizing the peak pressure and duration increased with increasing drop height and with increasing thickness. In the cylinder shape, it was confirmed that the duration was greater than deadrise angle of 10° due to the air effect. Also, the duration was greater than 3 mm at the thickness of 5 and 8 mm due to the air effect.

Figure 22 shows the peak pressures by the bottom thickness and drop height. The dead-rise angle of 10 degrees in the model means that that the measured pressure is significantly lower than the cylinder shape. This means that the cylindrical structure, which is typically used in the architecture and installation of marine structures, is under the greatest pressure from the phenomenon of slamming.

### 7. Conclusions

In this study, various free-drop experiments were performed using a steel model with a deadrise angle of 10° and a cylindrical model, which were dropped from heights of 1.0 and 1.7 m. The results are compared with those obtained by employing a rigid wooden model. The difference in results confirms the effect of elasticity of the material on the slamming load. The purpose of this experiment is to identify the pressure and behavioral characteristics of the model.

It was observed that the slamming load was greater in the case of the cylindrical model compared to the cases of the flat model and model with deadrise angle of  $10^\circ$ , as shown in Figure 22. A second peak was confirmed in the case of the model with a deadrise angle of  $10^\circ$ , occurring approximately 0.03 s after the first peak. This was confirmed by the theoretically calculated natural frequency of the structure (34.85 Hz) being very close to the experimentally obtained value (33.33 Hz). Additionally, the value obtained from the hammer test was 34.15 Hz, which was substantially similar to the experimental value. The second peak obtained was higher than the first peak. In the case of the cylindrical model and drop height of 1.7 m, it was observed that the first peak occurred at 0.60 s and the second peak occurred approximately 0.03 s after the first peak, i.e., at 0.63 s. Furthermore, this was confirmed by the theoretically calculated natural frequency of the structure (34.15 Hz) being very close to the experimentally obtained natural frequency (33.33 Hz). The value obtained from the hammer test was 35.5 Hz, which was substantially similar to the experimental value.

It was confirmed that even with a single wave, the impact pressure occurs several times according to the natural frequency of the structure. This means that the structure can be permanently damaged even by a single wave, and fatigue failure can occur due to repetitive slamming.

These results can resolve the lack of information on slamming loads. The results obtained in this study can aid in the development of design techniques; the effect of slamming pressure can be incorporated into the fundamental design of parameters to prevent structural damage.

Negative pressure occurs due to the elastic effect of the structure—it was confirmed that the duration of the pressure was longer. In addition, in the case of the cylindrical shape, the first peak is larger compared to other structures, but the size of the second peak tends to decrease. The study of slamming turns out to be an important factor to consider the elastic effects of the structures. It seems that the second peak pressure occurs when the negative pressure, due to the elastic effect, was close to  $-0.1$  Mpa.

These results are expected to be reflected in structural design via comparison with the peak width and natural frequency of the structure. Therefore, the design considering the elastic influence of the structure should be carried out and structural damage of offshore structures and floating offshore wind turbines are expected to be reduced.

The dynamic nonlinear analysis was performed using ABAQUS software. In the analysis, slamming loads obtained from the free-drop experiments were used, and the accuracy of the numerical prediction was acceptable, as seen from the experimental results.

However, further studies are needed to ensure accuracy and reliability, and additional experiments are required to be performed under the same conditions to ensure confidence in results.

**Author Contributions:** Conceptualization, validation, B.S. and H.S.; methodology, software, writing—original draft preparation, B.S.; writing—review and editing, supervision, H.S. All authors have read and agreed to the published version of the manuscript.

**Funding:** This research was supported by the Korea Institute of Energy Technology Evaluation and Planning (KETEP) grant funded by the Korea government (MOTIE) (20184030202280) and also by Korea Electric Power Corporation. (R18XA03).

**Conflicts of Interest:** The authors declare no conflict of interest. The funders had no role in the design of the study; in the collection, analyses, or interpretation of data; in the writing of the manuscript, or in the decision to publish the results.

## References

1. Kim, Y.J.; Shin, K.S.; Shin, C.H.; Kang, J.M.; Kim, M.S.; Kim, S.C.; Oh, S.G.; Rim, C.W.; Kim, D.H.; Kim, D.H.; et al. Prediction of Bow Flare Impact Pressure and Its Application to Ship Structure Design—Container Ship and PCC-. *J. Soc. Nav. Archit. Korea* **2003**, *40*, 29–36.
2. Kim, Y.J.; Shin, K.S.; Shin, C.H.; Kang, J.M.; Kim, M.S.; Kim, S.C.; Oh, S.G.; Rim, C.W.; Kim, D.H.; Kim, D.H.; et al. Prediction of Bow Flare Impact Pressure and Its Application to Ship Structure Design—Tanker and Bulk Carrier. *J. Soc. Nav. Archit. Korea* **2015**, *52*, 418–424. [[CrossRef](#)]

3. Chuang, S.-L. Investigation of Impact of Rigid and Elastic Bodies with Water. 1970. Available online: <https://www.semanticscholar.org/paper/INVESTIGATION-OF-IMPACT-OF-RIGID-AND-ELASTIC-BODIES-Chuang/5412f85ca28d037d14df0e8b3052280dd6b21968> (accessed on 22 February 2020).
4. Faltinsen, O.M. Water Entry of a Wedge with Finite Deadrise Angle. *J. Ship Res.* **2002**, *46*, 39–51.
5. Shin, H.; Seo, B.; Cho, S.R. Experimental investigation of slamming impact acted on flat bottom bodies and cumulative damage. *Int. J. Nav. Archit. Ocean Eng.* **2018**, *10*, 294–306. [[CrossRef](#)]
6. Cho, S.R.; Choi, S.I.; Son, S.K. Dynamic material properties of marine steels under impact loadings. In Proceedings of the 2015 World Congress on Advances in Structural Engineering and Mechanics, Incheon, Korea, 25–29 August 2015.
7. Yamamoto, Y.; Iida, K.; Fukasawa, T.; Murakami, T.; Arai, M.; Ando, A. Structural damage analysis of a fast ship due to bow flare slamming. *Int. Shipbuild. Prog.* **1985**, *32*, 124–136. [[CrossRef](#)]
8. Laur, U.; Lehtola, K.; Eksborh, A.L. *Final Report on the Capsizing on 28 September 1994 in the Baltic Sea of the Ro-Ro Passenger Vessel MV Estonia, Extreme Environmental Events Complexity in Forecasting and Early Warning*; Edita Publishing Ltd.: Helsinki, Finland, 1997; p. 228.
9. Buchner, B.; Voogt, A. Wave impacts due to steep fronted waves. In Proceedings of the Rogue Waves, Brest, France, 20–22 October 2004; p. 7.
10. The United Kingdom Merchant Shipping. *Marine Accident Investigation Branch, Southampton United Kingdom*; Napoli Report No 9/2008; The United Kingdom Merchant Shipping: UK, 2008.
11. Kleefsmann, T. Water Impact Loading on Offshore Structures A Numerical Study. 2005. Available online: <http://citeseerx.ist.psu.edu/viewdoc/download?doi=10.1.1.211.8751&rep=rep1&type=pdf> (accessed on 22 February 2020).
12. Zhao, R.; Faltinsen, O.; Aarsnes, J. Water Entry of Arbitrary Two-Dimensional Sections with and without Flow Separation. In Proceedings of the 21st Symposium on Naval Hydrodynamics, Trondheim, Norway, 19 August 1997.
13. Dobrovolskaya, Z.N. On some problems of similarity flow of fluid with a free surface. *J. Fluid Mech.* **1969**, *36*, 805–829. [[CrossRef](#)]
14. Mei, X.; Liu, Y.; Yue, D.K.P. On the water impact of general two-dimensional sections. *Appl. Ocean Res.* **1999**, *21*, 1–15. [[CrossRef](#)]
15. De Backer, G.; Vantorre, M.; Beels, C.; De Pré, J.; Victor, S.; De Rouck, J.; Van Paepegem, W. Experimental investigation of water impact on axisymmetric bodies. *Appl. Ocean Res.* **2009**, *31*, 143–156. [[CrossRef](#)]
16. Faltinsen, O.; Kjaerland, O.; Nøttveit, A.; Vinje, T. Water Impact Loads And Dynamic Response Of Horizontal Circular Cylinders in Offshore Structures. In Proceedings of the Offshore Technology Conference, Houston, TX, USA, 2–5 May 2008.
17. Sun, H.; Faltinsen, O.M. Water impact of horizontal circular cylinders and cylindrical shells. *Appl. Ocean Res.* **2006**, *28*, 299–311. [[CrossRef](#)]
18. Wienke, J.; Oumeraci, H. Breaking wave impact force on a vertical and inclined slender pile-Theoretical and large-scale model investigations. *Coast. Eng.* **2005**, *52*, 435–462. [[CrossRef](#)]
19. Faltinsen, O.M.; Kvålsvold, J.; Aarsnes, J.V. Wave impact on a horizontal elastic plate. *J. Mar. Sci. Technol.* **1997**, *2*, 87–100. [[CrossRef](#)]
20. Iafrati, A.; Korobkin, A.A. Hydrodynamic loads during early stage of flat plate impact onto water surface. *Phys. Fluids* **2008**, *20*, 082104. [[CrossRef](#)]
21. Van Nuffel, D.; Vepa, K.S.; de Baere, I.; Degrieck, J.; de Rouck, J.; van Paepegem, W. Study on the Parameters Influencing the Accuracy and Reproducibility of Dynamic Pressure Measurements at the Surface of a Rigid Body During Water Impact. *Exp. Mech.* **2013**, *53*, 131–144. [[CrossRef](#)]
22. PCB Piezotronics. Technical Sheet of Pressure Transducer of Type 102B06. Available online: [http://www.pcb.com/contentstore/docs/PCB\\_Corporate/Pressure/products/Manuals/102B06.pdf](http://www.pcb.com/contentstore/docs/PCB_Corporate/Pressure/products/Manuals/102B06.pdf) (accessed on 22 February 2020).
23. ASTM E8/E8M. *Standard Test Methods for Tension Testing of Metallic Materials*; ASTM E8/E8M: West Conshohocken, PA, USA, 2011.
24. Villavicencio, R.; Soares, C.G. Numerical modelling of the boundary conditions on beams struck transversely by a mass. *Int. J. Impact Eng.* **2011**, *38*, 384–396. [[CrossRef](#)]
25. Seo, B.; Truong, D.D.; Cho, S.; Kim, D.; Park, S.; Shin, H. A study on accumulated damage of steel wedges with dead-rise 10° due to slamming loads. *Int. J. Nav. Archit. Ocean Eng.* **2018**, *10*, 520–528. [[CrossRef](#)]

26. Haugen, E.M. *Hydro Elastic Analysis of Slamming on Stiffened Plates with Application to Catamaran Wetdecks*; Norwegian University of Science and Technology: Trondheim, Norway, 1999.
27. Frieze, P.A.; Paik, J. Are classification society-based standards appropriate for designing ship structures. In Proceedings of the RINA, Royal Institution of Naval Architects International Conference-Developments in Classification and International Regulations-Papers, London, UK, 24–25 January 2007.
28. Engle, A.; Lewis, R. A comparison of hydrodynamic impacts prediction methods with two dimensional drop test data. *Mar. Struct.* **2003**, *16*, 175–182. [[CrossRef](#)]
29. Sinha, S.; Kar, S.; Sarangdhar, D.G. Development of Simplified Structural Design Formulation for Slamming Loads. In Proceedings of the ASME 2008 27th International Conference on Offshore Mechanics and Arctic Engineering. American Society of Mechanical Engineers Digital Collection, Mumbai, India, 27 July 2009.



© 2020 by the authors. Licensee MDPI, Basel, Switzerland. This article is an open access article distributed under the terms and conditions of the Creative Commons Attribution (CC BY) license (<http://creativecommons.org/licenses/by/4.0/>).